Protein Science (1995), *4*:1045–1055. Cambridge University Press. Printed in the USA.

Characterization of the N-terminal half-saturated state of calbindin D_{9k}: NMR studies of the N56A mutant

BRIAN WIMBERLY,[1] EVA THULIN,[2] AND WALTER J. CHAZIN[1]

[1] Department of Molecular Biology, The Scripps Research Institute, La Jolla, California 92037
[2] Department of Physical Chemistry 2, The Chemical Centre, University of Lund, S-221 00 Lund, Sweden

(RECEIVED December 14, 1994; ACCEPTED April 3, 1995)

Abstract

Calbindin D_{9k} is a small EF-hand protein that binds two calcium ions with positive cooperativity. The molecular basis of cooperativity for the binding pathway where the first ion binds in the N-terminal site (I) is investigated by NMR experiments on the half-saturated state of the N56A mutant, which exhibits sequential yet cooperative binding (Linse S, Chazin WJ, 1995, *Protein Sci 4*:1038–1044). Analysis of calcium-induced changes in chemical shifts, amide proton exchange rates, and NOEs indicates that ion binding to the N-terminal binding loop causes significant changes in conformation and/or dynamics throughout the protein. In particular, all three parameters indicate that the hydrophobic core undergoes a change in packing to a conformation very similar to the calcium-loaded state. These results are similar to those observed for the $(Cd^{2+})_I$ state of the wild-type protein, a model for the complementary half-saturated state with an ion bound in the C-terminal site (II). Thus, with respect to cooperativity in either of the binding pathways, binding of the first ion drives the conformation and dynamics of the protein far toward the $(Ca^{2+})_2$ state, thereby facilitating binding of the second ion. Comparison with the half-saturated state of the analogous E65Q mutant confirms that mutation of this critical bidentate calcium ligand at position 12 of the consensus EF-hand binding loop causes very significant structural perturbations. This result has important implications regarding numerous studies that have utilized mutation of this critical residue for site deactivation.

Keywords: calbindin D_{9k}; calcium binding; cooperativity; mutation; NMR

The calcium ion has an important biological role as a second messenger in the regulation of a wide variety of cellular processes (Rasmussen, 1986a, 1986b, 1989). Regulatory calcium binding proteins (CaBPs) typically bind calcium only upon elevation of the local calcium concentration after a stimulatory influx of calcium ions. Ion binding to these proteins is believed to cause dramatic conformational changes that initiate further cellular responses. Many other CaBPs with a wide range of calcium affinities have been discovered, and in addition to calcium signaling, roles in calcium homeostasis, buffering, and transport have been implicated.

The majority of CaBPs belong to the calmodulin superfamily, which is characterized by the presence of one or more pairs of a helix-loop-helix binding motif termed the EF-hand (Kretsinger & Nockolds, 1973) and a conserved sequence in the binding loops. Structural studies of several of these proteins have shown that pairs of EF-hands pack in a parallel fashion to form a discrete globular domain, with a short β-type interaction between the binding loops. Despite extensive structural study, many questions remain concerning structure–function relationships in EF-hand CaBPs. In particular, the conformational consequences of calcium binding had not been directly determined at high resolution until the solution structures of the apo and calcium-loaded states of calbindin D_{9k} became available (Kördel et al., 1993; Skelton et al., 1994, 1995). Accompanying studies of protein dynamics have also revealed substantial reduction in flexibility on both fast and slow time scales as Ca^{2+} is bound (Skelton et al., 1992; Akke et al., 1993).

Calbindin D_{9k} is a small (75-residue) EF-hand CaBP thought to aid the absorption of calcium ions from the intestinal brush border membrane or possibly to act as an intracellular calcium buffer (Christakos et al., 1989; Staun, 1991). The protein consists of a single pair of EF-hands connected by a short linker loop (Fig. 1; Kinemage 1). The N-terminal EF-hand has a variant 14-residue ion-binding loop characteristic of the S-100 subfamily of CaBPs. Because of its small size, high thermal stability, and high solubility, calbindin D_{9k} has been an ideal system for detailed study of structure–function relationships in EF-hand pro-

Reprint requests to: Walter J. Chazin, T.S.R.I..-MB2, 10666 North Torrey Pines Road, La Jolla, California 92037; e-mail: chazin@scripps.edu.

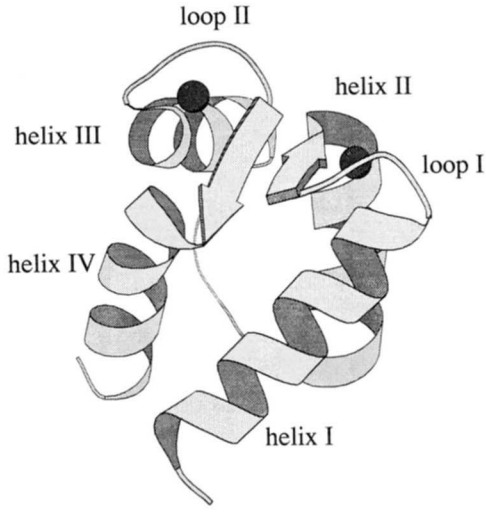

Fig. 1. Ribbon diagram (Kraulis, 1991) of the three-dimensional solution structure of calcium-loaded calbindin D_{9k} (Kördel et al., 1993; Brookhaven Protein Data Bank, accession number 2BCA).

teins using NMR and other biophysical methods (Forsén et al., 1993). The calcium affinities of the two binding loops in calbindin D_{9k} are high and very similar, and the protein exhibits positive cooperativity in the binding of calcium (Linse et al., 1987).

The molecular mechanism for cooperativity in calcium binding is an important but not fully understood aspect of structure–function relationships in EF-hand CaBPs. The available data for calbindin D_{9k} suggest that changes in protein conformation and dynamics upon binding of the first calcium ion make a substantial contribution to cooperativity (e.g., Akke et al., 1991, 1993, 1995; Skelton et al., 1992). Because the two EF-hands are not identical, there are two distinct binding pathways, one corresponding to binding of the first ion in the N-terminal site (I) and the other corresponding to the first ion binding in the C-terminal site (II). The cooperative free energy, ΔG^0_{coop}, is defined by the difference of the affinities of one site in the presence and absence of an ion in the other site:

$$\Delta G^0_{coop} = \Delta G^0(\mathrm{II,I}) - \Delta G^0(\mathrm{II}) = -RT\ln(K_{\mathrm{II,I}}/K_{\mathrm{II}})$$
$$= \Delta G^0(\mathrm{I,II}) - \Delta G^0(\mathrm{I}) = -RT\ln(K_{\mathrm{I,II}}/K_{\mathrm{I}}),$$

where the equilibrium constants are the site-binding constants defined in Figure 1 of the accompanying paper (Linse & Chazin, 1995).

A detailed understanding of the molecular basis for the cooperativity of calcium binding by calbindin D_{9k} requires the determination of the changes in conformation and dynamics that occur as each ion is bound. Though high-resolution structures and dynamic behavior have been reported for the apo and $(Ca^{2+})_2$ end states, studies of the $(Ca^{2+})_1$ [I] and $(Ca^{2+})_1$ [II] half-saturated states of wild-type protein are precluded by the similarity of the two site-binding constants (Linse et al., 1987). These states can only be studied indirectly, using model ion–protein systems in which one of the two site-binding constants is considerably reduced. A model for the site [II] half-saturated state has been examined in detail by taking advantage of the much greater affinity for Cd^{2+} of the C-terminal EF-hand versus the N-terminal EF-hand (Akke et al., 1991, 1995). A model for the $(Ca^{2+})_1$ [I] state was prepared by mutating the bidentate calcium ligand Glu 65 to Gln (E65Q) (Kinemage 3), which dramatically reduces the C-terminal site binding constant (Carlström & Chazin, 1993). A comparison of these $(Ca^{2+})_1$ [I] and $(Cd^{2+})_1$ [II] models revealed significant differences in both the flexibility and the conformation of the two half-saturated states and suggested a distinct asymmetry in the structural basis for cooperativity in the two binding pathways.

To validate the results obtained for $(Ca^{2+})_1$ E65Q [I] and the conclusions drawn from comparisons to the $(Cd^{2+})_1$ [II] state, the analogous mutant, N56A[3] (Kinemage 3), has been prepared. The companion paper (Linse & Chazin, 1995) describes a range of binding studies that permit identification and measurement of the free energy coupling between the two calcium binding sites. Here we report an in-depth characterization by NMR spectroscopy of the apo, $(Ca^{2+})_1$[I], and $(Ca^{2+})_2$ states of the N56A mutant of calbindin D_{9k}. Together, these results validate $(Ca^{2+})_1$[I]·N56A and $(Cd^{2+})_1$ [II] as models for the two half-saturated states of the wild-type protein. Furthermore, the comparative analysis of E65Q and N56A reveals that the $(Ca^{2+})_1$[I]·E65Q model is defective. This has important general implications regarding a wide range of studies of various CaBPs that have utilized analogous mutations of the conserved bidentate Glu ligand.

Results

Titration of N56A with Ca^{2+}

The measurement of calcium binding properties of the N56A mutant of calbindin D_{9k} is the subject of the accompanying paper (Linse & Chazin, 1995). A description of the Ca^{2+} titration is given here to set the stage for the detailed ^{1}H NMR analysis. Addition of calcium chloride to apo N56A results in the appearance of a second set of peaks in slow exchange with the apo state. During the first half of the titration, the linewidths were found to be very broadened (cf. Fig. 2 of the accompanying paper), presumably due to exchange of calcium between the $(Ca^{2+})_1$ and apo species. As the total amount of added calcium approaches 1 molar equivalent, the resonances become narrower, but also begin to shift with additional calcium, indicating fast exchange between the $(Ca^{2+})_1$ and $(Ca^{2+})_2$ species. Once approximately 2.5 molar equivalents of calcium have been added, the lines no longer shift, indicating that the second calcium binding loop has been filled. A small amount of precipitate was observed to form during the course of the titration.

In fact, the N56A mutation does not reduce the site II binding constant (Linse & Chazin, 1995) sufficiently to allow preparation of a pure $(Ca^{2+})_1$ sample: at 1 molar equivalent of added Ca^{2+}, significant amounts of all three states of the pro-

[3] Slow *cis–trans* isomerization about the Gly 42–Pro 43 peptide bond gives rise to two discrete sets of signals in the NMR spectrum (Chazin et al., 1989). In order to avoid this complication, the protein has been mutated at position 43 (e.g., P43G, P43M). These mutants have been examined extensively and do not exhibit any large changes in structure or calcium-binding properties relative to the wild-type protein (Kördel et al., 1990). To facilitate the discussion, P43M will be referred to as wild-type protein and the P43M label will usually be omitted when reference is made to either the E65Q, P43M or the N56A, P43M mutants.

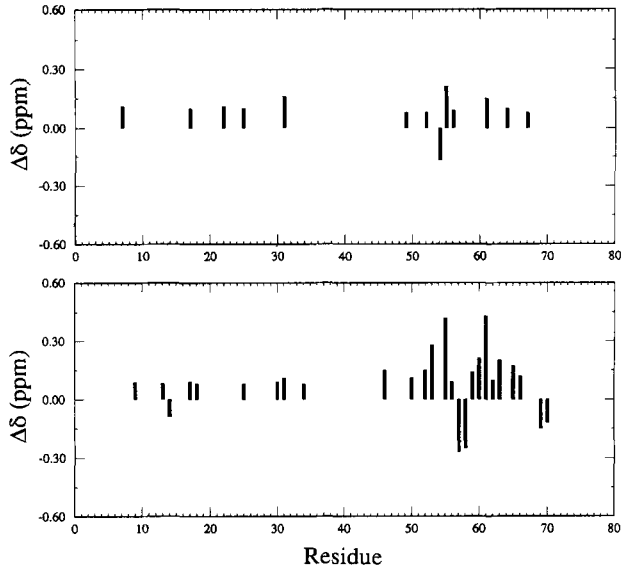

Fig. 2. Comparison of the backbone C^{α} (top) and amide (bottom) proton chemical shifts of the $(Ca^{2+})_2$ states of N56A and wild-type (P43M) calbindin D_{9k}. The differences in chemical shift difference between the apo and $(Ca^{2+})_2$ states ([$(Ca^{2+})_2$ – apo] – [$(Ca^{2+})_2$N56A – apoN56A]) are plotted. Only statistically significant differences ($\geq \pm 0.08$ ppm) are shown.

tein (apo, $(Ca^{2+})_1$, and $(Ca^{2+})_2$) are present in solution. From the perspective of limiting contamination by $(Ca^{2+})_2$ protein, it is desirable to stop the titration somewhat before 1 molar equivalent of calcium is added. However, if much less than 1 equivalent is added, the linewidths are too broad to allow the acquisition of high-quality spectra. Thus, our working conditions represent a compromise between these conflicting goals. Analysis of the chemical shift titration curves indicated that there is approximately 20% $(Ca^{2+})_2$ species present in the "$(Ca^{2+})_1$" sample as well as ca. 2% apo.

The apo and $(Ca^{2+})_2$ states of N56A

The first step in the analysis of a binding-site mutant is verification that the system is a viable model for the wild-type protein, which requires characterization of the Ca^{2+}-free and Ca^{2+}-loaded endstates. The chemical shifts of apo N56A were sufficiently similar to those of the wild-type protein (Skelton et al., 1990) to allow assignment of almost all backbone and many aromatic and methyl proton resonances by direct comparison of the fingerprint regions of their COSY spectra. These tentative assignments were confirmed, and additional assignments were made, via analysis of sequential connectivities in the NOESY spectrum. The statistically significant differences between the backbone chemical shifts of apo N56A and wild-type protein are reported in Table 1. Most of these are barely outside of the experimental error and can be attributed to the inability to make the experimental conditions exactly identical. Substantial differences in the backbone proton chemical shifts (>0.1 ppm) are observed only in the vicinity of the mutation. Because the chemical shift parameter is very sensitive to conformation and dynamics, the great similarity of virtually all backbone and side-chain methyl/aromatic proton chemical shifts indicates that the N56A mutation causes only very minimal and highly localized perturbations of the apo state.

Spectra of the $(Ca^{2+})_2$ states of N56A are also very similar to those of the wild-type protein, although less so than for the apo state. Approximately 60% of the backbone and most methyl and aromatic proton resonances could be tentatively assigned simply by comparison. These initial assignments were confirmed by connectivities observed to the side-chain protons in 2D scalar-correlated spectra (COSY, 2Q, TOCSY) and by sequential NOEs. Several iterations of tentative assignment and confirmation from sequential NOEs and/or side-chain scalar correlations were made until assignments for virtually all backbone and most side-chain proton resonances were complete. A comparison of the backbone chemical shifts of the $(Ca^{2+})_2$ states of N56A and wild-type protein is shown in Figure 2, represented as the δ(N56A) – δ(wild type) after normalization for the chemical shifts of the respective apo states. Overall, there is a great similarity in backbone chemical shifts, with substantial chemical shift differences (>0.10 ppm) observed only for the $C^{\alpha}H$ resonances of K7, Q22, L31, D54, K55, and V61 and for the backbone NH resonances of L31, L46, F50, E52, L53, K55, G57, D58, G59, E60, V61, F63, E65, F66, L69, and V70. All of these large differences in chemical shift arise from protons that are spatially proximate to the mutation site. D54 and D58 are calcium ligands, so their chemical shifts are expected to be especially sensitive to small changes in conformation or dynamics caused by mutation of the intervening ligand N56. The smaller chemical shift differences observed for residues 14–26, in and adjacent to Loop I, arise as a byproduct of the contacts between the two calcium-binding loops (cf. Fig. 1). The general similarity in chemical shifts of the $(Ca^{2+})_2$ states also extends to side-chain proton resonances, even those that have substantial ring-current shifts. For example, the highest upfield-shifted methyl group, that of I73 C^{δ}, has a chemical shift that is identical within experimental error to that of the wild-type protein. The observed similarity of the

Table 1. *Backbone ^1H NMR chemical shift differences[a] of apo N56A calbindin D_{9k} relative to those of apo P43M (pH 6.0, 300 K)*

NH		Ha	
Residue	Δδ	Residue	Δδ
E11	−0.05	A14	−0.06
A14	0.07	K25	−0.05
A15	0.06	L31	−0.06
K16	0.06	A56*	0.44
G18	−0.06		
K25	−0.05		
L28	0.05		
K29	0.06		
E52	−0.10		
L53	−0.10		
A56*	0.16		
E60	−0.07		
S62	−0.08		

[a] Only the statistically significant values (P43M – N56A) with an absolute value greater than 0.04 ppm are listed.

chemical shifts supports the conclusion that the N56A substitution has virtually no effect on the conformation and dynamics of the calcium-loaded state of the protein, other than small perturbations in the vicinity of the mutation.

The $(Ca^{2+})_1$ state of N56A

Due to exchange broadening, spectra of the $(Ca^{2+})_1$ state were more difficult to analyze than those of the apo or $(Ca^{2+})_2$ states. Nonetheless, there is a substantial similarity in the chemical shifts of the $(Ca^{2+})_1$ and $(Ca^{2+})_2$ states, which allowed a significant number of tentative spectral assignments by direct comparison, especially in the N-terminal half of the molecule. The assignments generated by comparison were confirmed or rejected by the observation of the expected scalar correlations to the side chains and by sequential NOEs. The remaining assignments were made in the usual manner (e.g., Kördel et al., 1989), from an extensive analysis of all spectra. The ^1H chemical shift assignments for $(Ca^{2+})_1$ N56A are reported in Table 2.

To obtain insights into the dynamic and conformational changes caused by ion binding, the backbone chemical shift differences in N56A associated with the two binding steps, $[(Ca^{2+})_1 - \text{apo}]$, $[(Ca^{2+})_2 - (Ca^{2+})_1]$, have been analyzed (Fig. 3, top panels). In the N-terminal EF-hand, the backbone chemical shifts of the $(Ca^{2+})_1$ state are very close to those of the $(Ca^{2+})_2$ state. To a certain extent, this similarity is expected because the N-terminal binding site is filled. In the C-terminal EF-hand, the backbone amide chemical shifts in the $(Ca^{2+})_1$ state of a large fraction of the residues are intermediate between the apo and $(Ca^{2+})_2$ states, with apo-like shifts only for G59. However, the amide shifts for the C-terminus of helix IV (K71–Q75) are similar to those seen in the $(Ca^{2+})_2$ state. In addition, the $C^{\alpha}H$ chemical shifts of residues in the center of loop II (G59–S62) and the residues from the center of helix IV to the C-terminus (L69–Q75) are close to those seen in the $(Ca^{2+})_2$ state, whereas only the $C^{\alpha}H$ shifts from residues at the beginning and end of loop II are apo-like. In summary, there are large and widely dispersed chemical shift changes upon binding of the first ion (black bars), suggesting that both EF-hands experience significant changes in conformation and/or dynamics when site I is occupied. In contrast, the chemical shift changes induced by binding of the second ion (hatched bars) are smaller in magnitude and occur

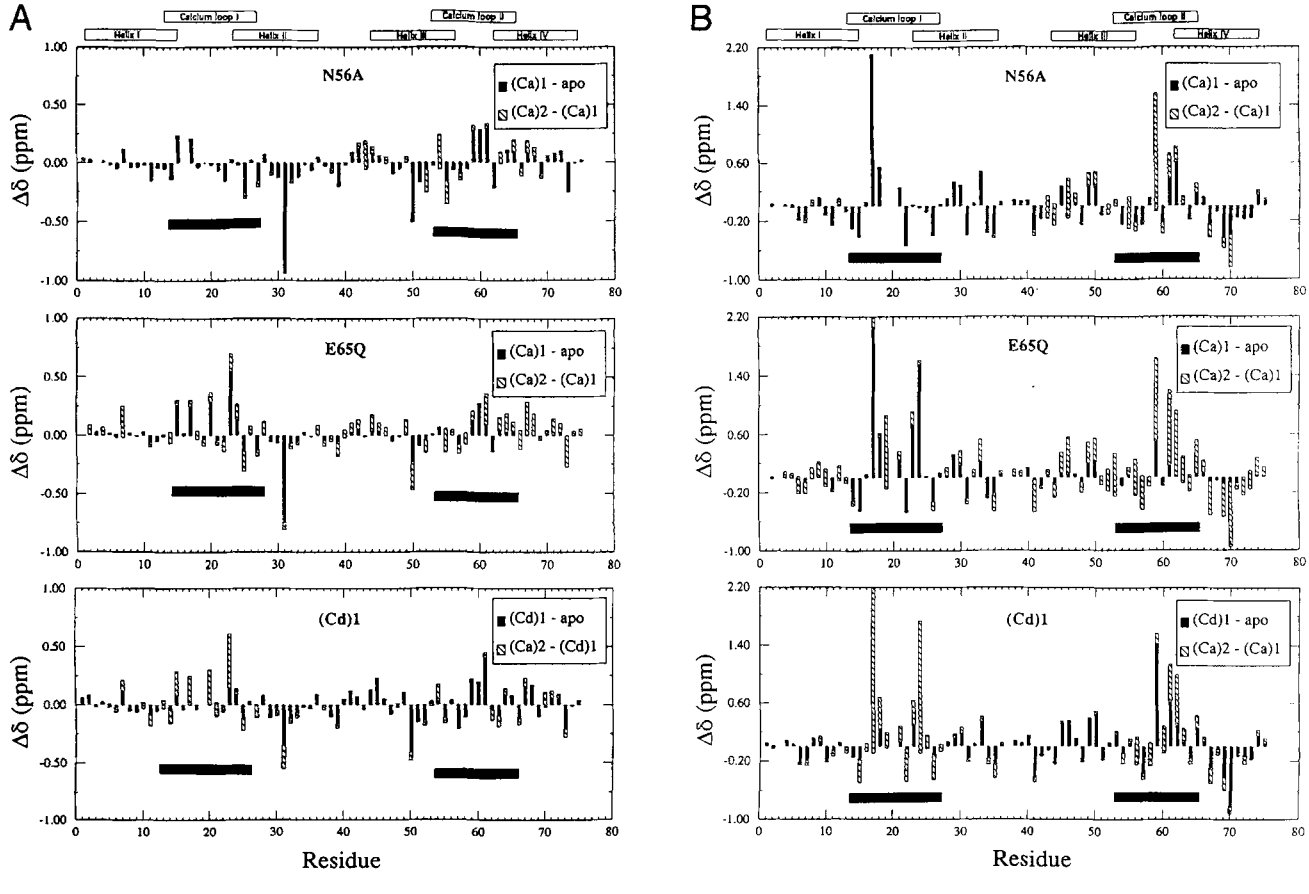

Fig. 3. Backbone C^{α} **(A)** and amide **(B)** proton chemical shift differences as a function of ion occupancy for N56A, E65Q, and wild-type [P43G] calbindin D_{9k}. Filled bars indicate the $(Ca^{2+})_1$ – apo differences; hatched bars indicate the $(Ca^{2+})_2 - (Ca^{2+})_1$ differences. Some of the differences for residues 20, 23, and 24 of N56A are not plotted because the necessary N56A apo assignments were not obtained. For the $(Ca^{2+})_2 - (Ca^{2+})_1$ E65Q data, P43M $(Ca^{2+})_2$ chemical shifts were used instead of E65Q $(Ca^{2+})_2$ chemical shifts because a $(Ca^{2+})_2$ state of E65Q could not be prepared (Carlström & Chazin, 1993). For the wild-type protein, the half-saturated state corresponds to one cadmium ion bound in site II. The locations of the helices and calcium binding loops are indicated schematically at the top of the figure. Within each panel, horizontal black bars highlight the calcium binding loops.

Table 2. *Proton chemical shift assignments for $(Ca^{2+})_1$ [I] N56A calbindin D_{9k} (pH 6.0, 300 K)*[a]

	NH	Hα	Hβ	Hγ	Hδ	Other
M0						
K1		4.55	1.83	1.59, 1.59	1.71	2.92
S2	9.02	4.74	4.44, 4.08			
P3		4.31	2.03, 2.47	2.24	3.73	
E4	8.76	4.07	1.97, 2.08	2.41		
E5	8.03	4.16	2.06, 2.27	2.42, 2.42		
L6	8.62	4.30	2.22, 1.78	1.90	1.02, 0.93	
K7	8.35	3.89	1.60, 1.84	0.80, 0.80	1.13	
G8	7.80	3.91, 3.91				
I9	7.97	3.88	2.20	1.99	0.98	1.16
F10	8.55	3.53	3.31, 2.83		6.49	7.07, 7.46
E11	8.56	3.76	1.91, 2.08	2.66		
K12	7.59	3.92	1.85, 1.77	1.12	1.47	
Y13	7.23	4.04	2.82, 2.39		7.47	6.78
A14	8.36	3.89	0.41			
A15	6.89	4.30	1.42			
K16	7.17	3.85	1.96, 2.09	1.49	1.69, 1.82	2.75, 2.75
E17	9.63	4.72	1.96, 1.87	2.09, 2.18		
G18	8.96	3.92, 3.68				
D19		4.71	2.66, 2.92			
P20		4.87	2.20	1.87, 2.06	3.99	
N21	9.10	4.99	2.67, 3.01			
Q22	7.23	5.02	1.61, 1.97	2.10, 2.21		
L23	9.74	5.39	1.83, 1.71	1.38	0.43, 0.57	
S24	10.13	4.98	4.37, 4.12			
K25	8.72	3.50				
E26	8.10	3.94	1.93	2.22, 2.32		
E27	7.78	3.92	1.93,2 .26	2.36		
L28	8.73	4.04	2.24	1.68	1.07, 1.07	
K29	8.38	3.68	2.02, 1.83	1.40	1.65	2.96, 2.96
L30	7.53	4.02			1.01, 1.01	
L31	8.11	2.27	1.81		0.93, 0.98	
L32	8.84	3.90	1.97, 1.33	2.20	0.95, 1.14	
Q33	8.47	3.85	1.98, 2.15	2.34, 2.49		
T34	7.62	4.06	4.38	1.28		
E35	8.49	4.22	1.43, 1.51	2.35		
F36	7.84	5.18	2.78, 3.36		7.16	7.02, 7.24
P37		4.21	2.47			
S38	8.40	4.29	4.00, 3.91			
L39	7.94	4.21	1.75, 1.90		0.72, 0.72	
L40	7.68	4.33	1.65, 1.90	1.49	0.90, 0.81	
K41	7.57	4.31	1.76, 1.91	1.38, 1.47		3.01, 3.01
G42	8.05	4.18, 3.90				
M43	8.00	4.68	(2.09)	2.63, 2.58		
S44	8.57	4.58	3.85, 3.85			
T45	8.05	4.39	4.47	1.29		
L46	8.01	4.07	1.80	(1.95)	0.97, 0.97	
D47	8.24	4.19	2.77, 2.56			
E48	7.74	4.02	2.17	2.32, 2.32		
L49	8.10	4.11	1.65, 1.55	1.63	0.72, 0.78	
F50	8.65	3.71	3.04, 3.19		7.15	7.15, 7.15
E51	7.86	3.99	2.11	2.47, 2.47		
E52	7.81	4.04	2.13	2.01, 2.30		
L53	7.87	4.14	1.15, 1.65	1.92	0.73, 0.80	
D54	8.00	4.41	2.57, 2.69			
K55	8.08	4.10	1.64	1.74	3.10, 3.10	
A56	7.83	4.28	1.49			
G57	7.84	3.92, 3.92				
D58	8.49	4.67	2.62, 2.91			
G59	8.72	4.38, 3.49				
E60	7.82	5.13	1.64, 1.99	2.17		
V61	9.55	5.02	2.36	1.04, 0.57		
S62	9.34	4.84	4.49, 4.21			
F63	9.36	3.38	2.55, 2.26		6.65	7.12, 7.35
E64	8.52	3.79	1.87, 2.03	2.30		
E65	7.68	4.15	1.77	2.42		
F66	8.82	4.07	3.27, 3.16		7.01	7.16, 7.24
Q67	7.87	3.30	1.91, 1.94	2.17, 2.35		
V68	7.07	3.49	2.07	0.82, 0.98		
L69	7.13	3.73	1.34, 1.20	1.38	0.60, 0.71	
V70	7.59	3.16	1.85		0.51, 0.68	
K71	7.43	3.97	1.75, 1.81	1.41	1.61	2.91, 2.91
K72	7.51	4.15	1.85, 1.85	1.49	1.46, 1.46	2.72, 2.83
I73	7.42	4.07	1.79	0.92, 1.23	0.30	0.64
S74	7.68	4.49	3.82, 3.82			
Q75	7.61	4.15	2.03, 2.09	2.31, 2.31		

[a] Values in parentheses are tentative.

almost exclusively in the C-terminal EF-hand, which is indicative of only localized changes.

Further insight into the changes caused by ion binding was obtained from analysis of side-chain chemical shifts. In general, side-chain resonances experience larger changes upon binding of the first ion versus the second ion, just as observed for the backbone $C^{\alpha}H$ and NH resonances. As expected, binding of the first ion induces large changes in the side-chain residues of the N-terminal calcium-binding loop. Less dramatic effects are seen not only in the remainder of the N-terminal EF-hand, but also in the C-terminal calcium-binding loop and in helix IV.

The effects on chemical shifts in helix IV are most interesting, as these have been correlated with specific changes in the structure upon ion binding. From the comparison of the three-dimensional structures of the apo and $(Ca^{2+})_2$ proteins (Skelton et al., 1994, 1995), certain of these side-chain chemical shifts (in particular, the upfield-shifted methyl resonances of V70 and I73) have been identified as diagnostic of a reorganization of the hydrophobic core. To provide further insight, Table 3 lists the side chain chemical shifts for all residues in helix IV. Among these residues, the side chains of L69, V70, and I73 are found to experience particularly large ion-induced changes in chemical shift. For these and most others, the chemical shifts in the $(Ca^{2+})_1$ state are almost indistinguishable from those in the $(Ca^{2+})_2$ state. Thus, binding of the first ion drives helix IV to a $(Ca^{2+})_2$-like state wherein the hydrophobic core is similar to that observed upon full loading of the wild-type protein.

The conformation of the hydrophobic core in the $(Ca^{2+})_1$ [I] state was also probed more directly by an analysis of characteristic NOEs. On the basis of the known differences between the apo and calcium-loaded states, a number of long-range NOEs have been identified as diagnostic of either the apo-like or the $(Ca^{2+})_2$-like packing of the hydrophobic core. The largest differences between the apo and $(Ca^{2+})_2$ states of calbindin D_{9k} occur in helix IV, in particular as regards the packing of the hydrophobic core in the region near the C-terminal half of helix IV and the C-terminus of helix II (Fig. 4; Kinemage 2). For example, in the apo state (blue), the side-chain of Val 70 is packed against the aromatic ring of Phe 36, and NOEs are observed between the two side chains. Reorganization of the hydrophobic core upon Ca^{2+} binding results in an exchange of the Val 70 and Ile 73 side chains in the pocket under Phe 36; hence, in the $(Ca^{2+})_2$ state (red), NOEs are observed between Phe 36 and Ile 73, but not between Phe 36 and Val 70. This change in conformation is also reflected in the large changes in the ring-current-induced chemical shifts observed for the methyl protons of Val 70 and Ile 73 described above.

The NOESY spectra of $(Ca^{2+})_1 \cdot$N56A were examined for the presence or absence of these diagnostic NOEs, in an attempt to assess whether the hydrophobic core of the half-saturated state was more apo-like or $(Ca^{2+})_2$-like. The NOEs between Phe 36 and Val 70 or Ile 73 (discussed above) are the easiest to interpret. In $(Ca^{2+})_1 \cdot$N56A, NOEs are observed between the F36 β, ϵ, and ζ protons and the I73 γ-methyl protons, as found in the $(Ca^{2+})_2$ state (cf. solid lines in Fig. 4). Other NOEs observed, such as F66 ϵ/I73 γ-methyl, are also indicative of a $(Ca^{2+})_2$-like core packing. This conclusion is corroborated further by the absence or greatly reduced intensity of NOEs diagnostic of the apo-like packing of the hydrophobic core (e.g., F36 ϵ/V70 γ-methyl; dashed lines). Thus, in accordance with the results of the comparison of chemical shifts, the NOE results indicate that the conformation of the hydrophobic core of the $(Ca^{2+})_1$ state is very similar to that of the $(Ca^{2+})_2$ state.

Information regarding protein dynamics can be obtained from an analysis of the rates of exchange of amide protons with solvent and of aromatic ring flip rates. In calbindin D_{9k}, the resonances of the C^{δ} protons of Phe 10 exhibit a substantial degree of exchange broadening in the $(Ca^{2+})_2$ state due to a reduced rate of flipping of the aromatic ring. The packing in the apo protein is apparently more flexible, as the corresponding resonance lines are narrow. This difference in flexibility is likely to contribute to the observed changes in the chemical shifts of the Phe 10 protons upon ion binding. In N56A, the resonance lines are narrow in the apo state and exchange broadened in the $(Ca^{2+})_1$ and $(Ca^{2+})_2$ states. Moreover, the chemical shifts of the $(Ca^{2+})_1$ and $(Ca^{2+})_2$ states are very similar to each other and to those of the $(Ca^{2+})_2$ state of the wild-type protein. Thus, the major portion of the change in Phe 10 ring dynamics is associated with binding of the first Ca^{2+} ion.

Amide proton exchange rates provide an indirect measure of protein dynamics on a relatively slow (>millisecond) time scale. These rates are particularly useful for the characterization of the absence or presence of hydrogen bonds, and to assess relative flexibility within or between various states of a protein (e.g., Wagner, 1983). A qualitative evaluation of the exchange rates in $(Ca^{2+})_1 \cdot$N56A (Fig. 5) reveals the characteristic pattern reflective of the primary elements of secondary structure. As observed in previous studies of calbindin D_{9k} (Skelton et al., 1992), the N-terminal half of the molecule appears to be inherently less flexible and exhibits fewer changes in exchange rate

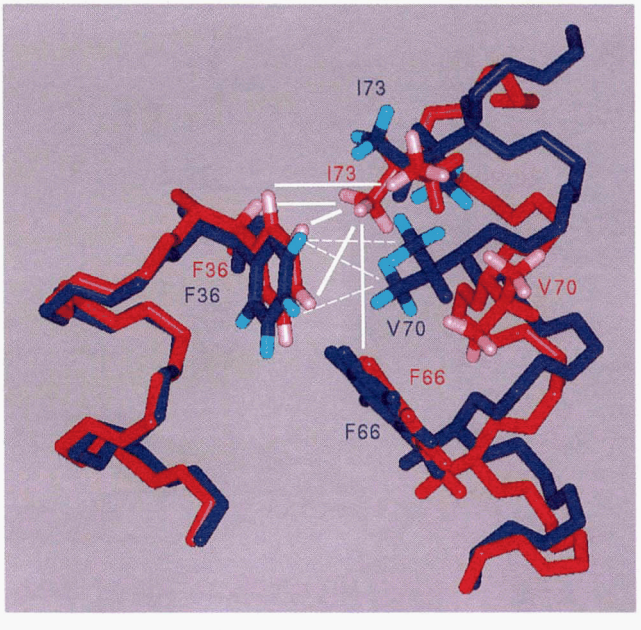

Fig. 4. NOEs diagnostic of the ion-induced change in packing of the hydrophobic core. Helix II from the solution structures of calcium-loaded (red; Kördel et al., 1993) and apo (blue; Skelton et al., 1995) calbindin D_{9k} were superimposed to reveal the different packing schemes adopted by helix IV in the two states. NOEs diagnostic of the $(Ca^{2+})_2$ and apo states are indicated by solid and dashed lines, respectively.

Table 3. *Chemical shifts of the side-chain protons of helix IV in the apo, half-saturated, and $(Ca^{2+})_2$ states of calbindin D_{9k}*

		Half-saturated			
	Apo	N56A	E65Q	$(Cd^{2+})_1$	$(Ca^{2+})_2$
Phe 63					
β, β'	2.59, 2.37	2.55, 2.26	2.54, 2.19	2.60, 2.30	2.68, 2.48
$\delta 1, \delta 2$	6.76, 6.76	6.65, 6.65	6.76, 6.76	6.58, 6.58	6.53, 6.53
$\epsilon 1, \epsilon 2$	7.15, 7.15	7.12, 7.12	7.15, 7.15	7.13, 7.13	7.15, 7.15
ζ	7.31	7.35	7.32	7.34	7.36
Glu 64					
β, β'	2.02, 1.91	2.03, 1.87	2.04, 1.90	2.04, 1.91	2.08, 1.92
γ, γ'	2.39, 2.26	2.30, (2.30)	2.34, 2.25	2.26, (2.26)	2.23, 2.23
Glu 65					
β, β'	2.37, 2.02	1.77	2.40, 2.03	1.87	
γ, γ'	2.42	2.59, 2.47	2.57, 2.41		
Phe 66					
β, β'	3.34, 3.20	3.27, 3.16	3.43, 3.26	3.28, 3.17	3.32, 3.16
$\delta 1, \delta 2$	7.11, 7.11	7.01, 7.01	7.11, 7.11	6.95, 6.95	6.95, 6.95
$\epsilon 1, \epsilon 2$	7.34, 7.34	7.16, 7.16	7.28, 7.28	7.20, 7.20	7.18, 7.18
ζ	7.20	7.24	7.18	7.13	7.12
Gln 67					
β, β'	1.73, 1.72	1.94, 1.91	1.78, 1.71	2.05, 1.86	1.96, 1.93
γ, γ'	1.66, 1.66	2.35, 2.17	1.71, 1.62	2.15	2.36, 2.17
Val 68					
β	2.16	2.07	2.21	2.00	1.97
γ, γ'	1.01, 0.87	0.98, 0.82	1.00, 0.85	1.01, 0.85	1.06, 0.86
Leu 69					
β, β'	1.72, 1.65	1.34, 1.20	1.86, 1.66	1.32,1.37	1.37
γ	1.67	1.38	1.56	1.28	1.30
$\delta 1, \delta 2$	0.86, 0.83	0.71, 0.60	0.90, 0.86	0.70, 0.59	0.73, 0.59
Val 70					
β	1.46	1.85	1.50	1.93	1.88
$\gamma 1, \gamma 2$	0.42, 0.05	0.68, 0.51	0.48, 0.10	0.76, 0.61	0.72, 0.56
Lys 71					
β, β'	1.86, 1.80	1.81, 1.75	1.85, 1.79	1.81, 1.75	1.86, 1.78
γ, γ'	1.47, 1.34	1.41	1.45, 1.33	1.46, 1.41	1.49, 1.42
δ, δ'	1.60	1.61	1.59, 1.59	1.61, 1.61	1.63, 1.63
ϵ, ϵ'	2.89	2.91, 2.91	2.88, 2.88	2.91, (2.91)	2.93, 2.93
Lys 72					
β, β'	1.92, 1.92	1.85, 1.85	1.91, 1.91	1.88, 1.83	1.86, 1.86
γ, γ'	1.53, 1.38	1.49	1.51, 1.36	(1.54), 1.46	1.60, 1.51
δ, δ'	1.59	1.46, 1.46	1.58, 1.58	1.59, 1.39	1.47, 1.47
ϵ, ϵ'	2.87	2.83, 2.72	2.86, 2.86	(2.82, 2.70)	2.85, 2.75
Ile 73					
β	2.02	1.79	2.00	1.74	1.79
$\gamma 1, \gamma 2$	1.30, 1.24	1.23, 0.92	1.30, 1.22	1.22, 0.82	1.19, 0.82
$\gamma(CH_3), \delta(CH_3)$	0.81, 0.47	0.64, 0.30	0.82, 0.46	0.64, 0.25	0.64, 0.30
Ser 74					
β, β'	3.88, 3.81	3.82, 3.82	3.88, 3.81	3.87, 3.87	3.90, 3.90

than the C-terminal half. However, the observed $(Ca^{2+})_1$ rates do not tend to fall midway between the corresponding rates in the apo and $(Ca^{2+})_2$ states, as observed for other half-saturated states (Akke et al., 1991; Carlström & Chazin, 1993), but rather there is an *apparent* uniform increase in the rates for the $(Ca^{2+})_1$ state. We attribute this effect to the larger resonance linewidths and correspondingly lower sensitivity in the spectra of $(Ca^{2+})_1 \cdot$N56A, the byproduct of intermediate exchange between the predominant $(Ca^{2+})_1$ state and the small equilibrium population of the $(Ca^{2+})_2$ state (see below).

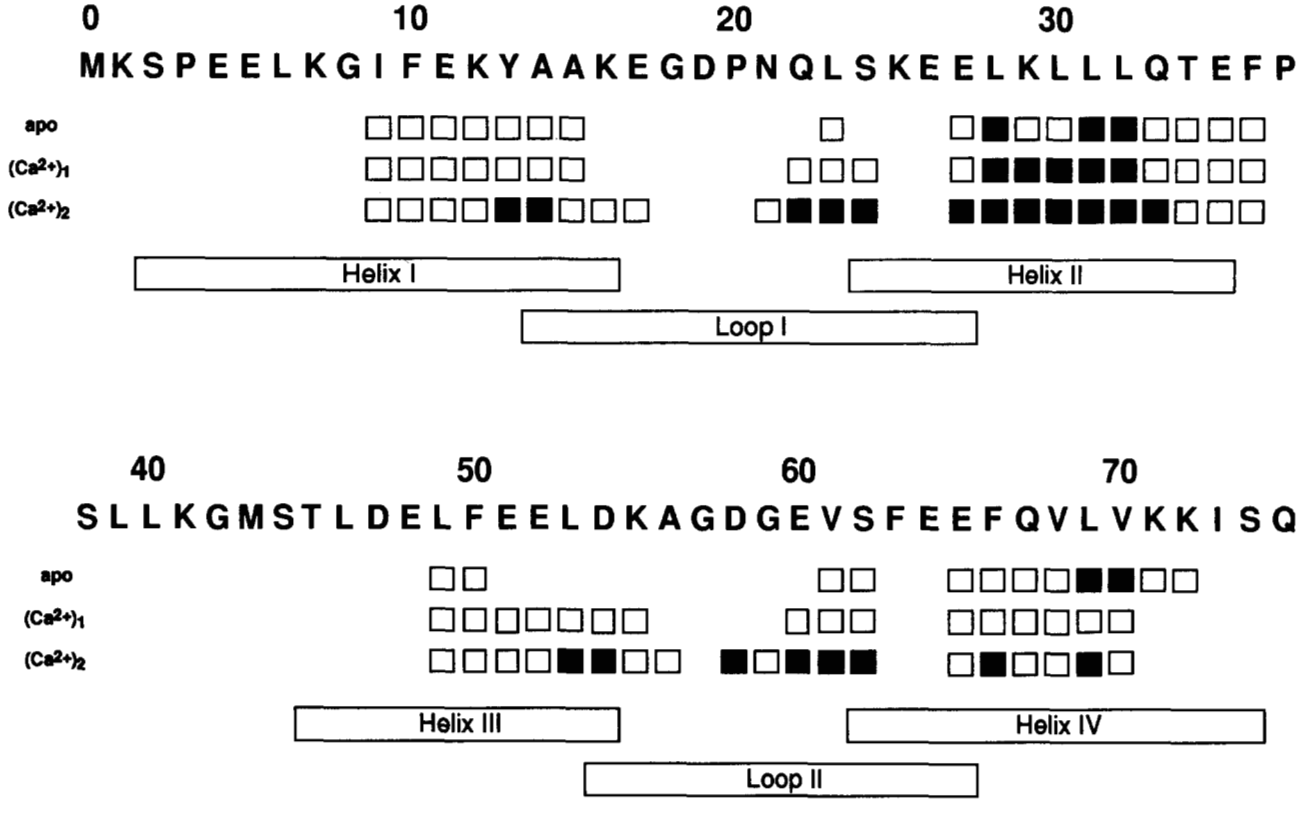

Fig. 5. Qualitative description of the rates of amide proton exchange in the apo, $(Ca^{2+})_1$ [I] N56A, and $(Ca^{2+})_2$ states of calbindin D_{9k}. The degree of shading in the boxes indicates the presence of an amide proton resonance in spectra recorded either 11 min (open boxes; $k_{ex} < 4.5 \times 10^{-3}$ s^{-1}) or 28 h (filled boxes; $k_{ex} < 3.0 \times 10^{-5}$ s^{-1}) after dissolution in ^2H_2O. The absence of a box indicates that the backbone amide proton could not be observed 11 min after dissolution in ^2H_2O ($k_{ex} > 4.5 \times 10^{-3}$ s^{-1}). The locations of the helices and calcium-binding loops are indicated at the bottom of the figure. The data for apo and $(Ca^{2+})_2$ P43G were taken from Skelton et al. (1992).

In contrast to the general trend observed in the backbone amide proton exchange rates of the $(Ca^{2+})_1$ state, the C-terminal portion of helix II and helix III exhibits a striking change in rates upon binding of the first ion. Interestingly, these are the amides that undergo the largest changes between the apo and $(Ca^{2+})_2$ states. For these residues, the behavior in the $(Ca^{2+})_1$ state is clearly closer to the $(Ca^{2+})_2$ state than the apo state. The results for helix III of N56A are in stark contrast to the apo-like amide proton exchange observed in $(Ca^{2+})_1$ [I] E65Q (cf. Fig. 8 of Carlström & Chazin, 1993). The observation of reductions in the rate of amide proton exchange not only in the loop where the ion is bound, but also for residues throughout the protein, is most informative. Clearly, the effects of binding the first ion in site I of calbindin D_{9k} are transmitted not only from the N-terminal binding loop to the C-terminal binding loop, but also to the hydrophobic core within and between the two EF-hands. These long-range effects on dynamics can be attributed to the site–site interactions that mediate the cooperativity in calcium binding.

Discussion

The N56A mutation was prepared as a complement to previous studies designed to characterize the half-saturated states of calbindin D_{9k}. Mutation in site II provides a model for the protein with a single Ca^{2+} ion bound in site I, $(Ca^{2+})_1$ [I]. Previously, we had studied the E65Q mutation (Carlström & Chazin, 1993), prompted by numerous reports of Glu → Gln mutations involving the highly conserved, bidentate Glu ligand in the 12th position of the consensus Ca^{2+} binding loop in other CaBPs (e.g., Beckingham, 1991; Haiech et al., 1991; Maune et al., 1992). As expected, and observed in other studies, this mutation was found to reduce very drastically the affinity for Ca^{2+} in site II in calbindin D_{9k}. However, although the objective of a "site deactivation" mutant is to disable the binding site without perturbing the essential interatomic interactions, we found that the affinity in site II was so drastically reduced that the site was never completely filled, even after addition of a large excess of calcium ions. But even more striking was the observation that the conformation corresponding to calcium-loaded state could not be attained. This raised a significant concern over the use of the Glu → Gln mutation; in an accurate model system the apo and $(Ca^{2+})_2$ endstates should bear a close resemblance to the wild-type protein.

The preparation and characterization of N56A was prompted by this uncertainty, as a means to test the hypotheses derived from the E65Q study. The selection of N56 for mutation was made on the basis of an examination of the calbindin D_{9k} structure, searching for a substitution that would reduce the affinity for calcium in site II without disrupting the $(Ca^{2+})_2$ structure.

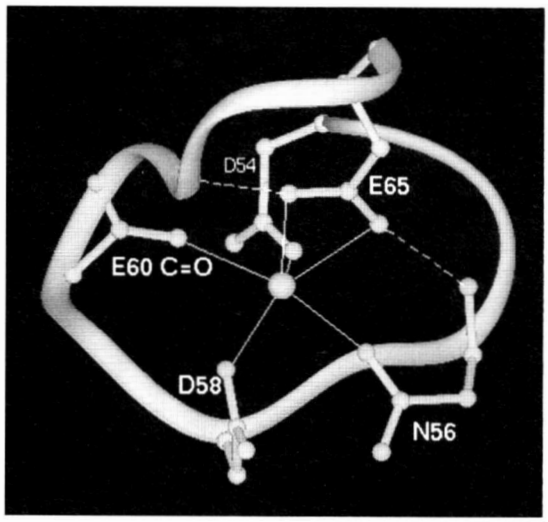

Fig. 6. C-terminal calcium-binding loop from the crystal structure of calcium-loaded calbindin D_{9k} (Svensson et al., 1992; Brookhaven Protein Data Bank, accession number 4ICB). Only the main- and side-chain ligands of the site II calcium ion are explicitly shown. Solid lines join the calcium ion and its six protein oxygen ligands (the seventh ligand, a water molecule, is hidden). Dashed lines indicate hydrogen bonds between the carboxylate oxygens of E65 and main-chain amide groups at each end of loop II. Note that the side chain of N56 is virtually free of interresidue contacts.

N56 corresponds to a conserved Asn or Asp residue that occupies the third position in the consensus Ca^{2+} binding loop and contributes the $+y$ calcium ligand (Szebenyi & Moffat, 1986; Strynadka & James, 1989). The advantages of the N56A substitution over E65Q are that the side chain of Asn 56 has few interactions with the remainder of the protein (Fig. 6; Kinemage 3), and a calcium-ligating oxygen atom is removed without changing the net charge of the protein. Putkey and coworkers have prepared analogous "site deactivation" mutations for studies of troponin C (Putkey et al., 1989). Comparison of the upper and middle panels of Figure 3 indicate that $(Ca^{2+})_2 \cdot$N56A is a much better model for the $(Ca^{2+})_2$ state of the wild-type protein than $(Ca^{2+})_2 \cdot$E65Q, and consequently, that N56A is a superior model system for the wild-type protein. Although similarity to wild type at the endpoints of the calcium binding pathway is not sufficient to guarantee the viability of the model for the half-saturated state, it does demonstrate that all of the interactions required to complete the binding process are present in N56A.

The changes in proton chemical shifts as a function of ion occupancy for N56A, E65Q, and Cd^{2+} binding by the wild-type protein are compared in Figure 3 and Table 3. For all three models, binding of the first ion (Fig. 3, filled bars) causes significant chemical shift changes in both EF-hands, suggesting widespread effects on conformation and/or dynamics. However, the magnitude of the changes that occur in the site that does not bind an ion is much *smaller* in E65Q than in $(Ca^{2+})_1 \cdot$N56A or the $(Cd^{2+})_1$ state of wild-type protein. Correspondingly, the response to binding of the second ion (Fig. 3, hatched bars) differs among the three models for half-saturated states. In N56A, binding of a second ion to the C-terminal site II results in significant changes in the backbone chemical shifts only for residues in the C-terminal EF-hand. Similarly, the changes in backbone chemical shift induced by binding of a second ion to the N-terminal site I of the $(Cd^{2+})_1$ protein are localized primarily to the N-terminal EF-hand. In E65Q, the changes in chemical shift between the $(Ca^{2+})_1$-state and the fully calcium-loaded protein occur not only in the N-terminal EF-hand where the second ion is binding but also in the C-terminal EF-hand. Thus, the conformational effects of binding of the second ion appear more extensive in the study of E65Q.

The explanation for the difference in behavior of the E65Q and N56A $(Ca^{2+})_1$ [I] models lies in the crucial structural role played by residue 65, the universally conserved bidentate Ca^{2+} ligand (Strynadka & James, 1989). The Glu → Gln substitution lowers the calcium affinity by removing one ligating oxygen atom and one negative charge from the protein. More importantly, however, the substitution also removes at least one of the hydrogen bonds between the E65 carboxylate oxygen atoms and backbone amide groups at both ends of the calcium binding loop (Fig. 6; Szebenyi & Moffat, 1986). These bridging hydrogen bonds appear to play an important role in stabilizing the correct overall conformation of the calcium binding loop (Strynadka & James, 1989). Thus, the Glu → Gln substitution at residue 12 of any EF-hand calcium binding loop not only drastically reduces the affinity for calcium but also significantly disrupts the structure of the calcium binding loop. For these reasons, we strongly advocate against the use of the Glu → Gln mutation of this highly conserved, bidentate Ca^{2+} ligand as a means to reduce binding affinity for probing the biochemical and biological significance of a binding event at a specific site.

Our results on calbindin D_{9k} suggest that disruption of even one of the bridging hydrogen bonds between the critical conserved Glu and other residues in the binding loop of the EF-hand has a significant effect not only on the free energy of binding, but also on the ability of the protein to attain the Ca^{2+}-loaded conformation. Consequently, effects from corresponding Glu → Gln mutations on assays of biological activity (e.g., Gao et al., 1993) may not be readily interpretable. What we do know is that there is a substantial perturbation of the communication between the two EF-hands, as reflected most clearly in the differences between the half-saturated states of N56A and E65Q, which must affect the cooperativity in the binding of calcium. The net increase in charge of the protein associated with the substitution of Gln for Glu is also expected to affect binding energetics and cooperativity. Although cooperative binding of calcium could conceivably be retained in mutants of the conserved bidentate Glu ligand, our results suggest that the molecular basis for cooperativity is likely to be altered.

Concluding remarks

The general conclusion from the analysis of structure and dynamics of the $(Ca^{2+})_1 \cdot$N56A model of the half-saturated state is that for the apo → $(Ca^{2+})_1$ [I] → $(Ca^{2+})_2$ pathway of ion binding, the conformation of the protein is driven almost completely to the $(Ca^{2+})_2$-state, far from the apo state. Figure 3 demonstrates that the calcium-induced chemical shift changes are on the whole far greater for the first binding step than the second. In addition, the observation of side-chain chemical shifts and NOEs diagnostic of a $(Ca^{2+})_2$-like core conformation strongly supports the conclusion that binding of a single calcium ion to site I induces a reorganization of the hydrophobic core to a con-

formation that closely resembles the fully Ca^{2+}-loaded protein. Amide proton exchange rates and the aromatic ring flip rates of Phe 10 indicate that the binding of the first ion causes significant changes in internal dynamics throughout the protein and drives the protein most of the way to the $(Ca^{2+})_2$ state. These observations closely parallel the results obtained in the study of $(Cd^{2+})_1$·calbindin D_{9k}, which modeled the apo → $(Ca^{2+})_1$ [II] → $(Ca^{2+})_2$ pathway of ion binding. Thus, on the basis of all available evidence from these models for the two complementary half-saturated states, it appears that both pathways of calcium binding have a half-saturated state of similar core conformation. This occurs despite the very clear differences in intrinsic features of the conformation, Ca^{2+} coordination, and certain aspects of the dynamics of the two EF-hands, and the corresponding asymmetry in their responses to ion binding (Skelton et al., 1992, 1994, 1995; Akke et al., 1993). Clearly, the energetic driving forces for Ca^{2+} binding must be distinctly different for the two binding pathways (Carlström & Chazin, 1993). These results provide strong motivation for continued efforts to identify the specific interactions providing communication between the paired EF-hands, as a means to determine the molecular basis for the cooperative binding of Ca^{2+} ions by EF-hand CaBPs.

Materials and methods

Sample preparation and calcium titration

A synthetic gene for the N56A, P43M double mutant of minor A bovine calbindin D_{9k} was constructed by cassette mutagenesis of the gene coding for the wild-type protein (Brodin et al., 1986). The protein was overexpressed from *Escherichia coli* strain MM 294 using the expression vector pRCB1 (Brodin et al., 1989) and purified as described previously (Johansson et al., 1990). The purified protein was stored at −20 °C as a lyophilized powder containing at least 2.5 molar equivalents of calcium.

For NMR experiments on the calcium-loaded state, 18 mg of this powder was dissolved in 0.42 mL of 90% H_2O/10% ^2H_2O and the pH adjusted to 6.0 with microliter additions of 0.1 M NaOH or 0.1 M HCl. For NMR experiments on the apo state, this sample was decalcified by adding 30 molar equivalents of disodium EDTA and raising the pH to 7.3, followed by ultrafiltration at 277 K using an Amicon 8 MC concentrator with a YM-2 membrane (MW cutoff of 2,000 Da) and a 3-atm excess pressure of argon. The sample volume was reduced from 2 mL to 0.3–0.5 mL 10 times. Water used to replenish the volume was pretreated with a Chelex column (Bio-Rad) to minimize its calcium content. The pH was adjusted to 6.0 for NMR experiments. The absence of upfield-shifted methyl resonances characteristic of the calcium-bound states indicated that there was negligible contamination of the apo sample by calcium. After completion of NMR experiments to obtain assignments of the apo state, a $(Ca^{2+})_1$ sample was prepared by titration with a 100 mM calcium chloride solution. Spectral changes were monitored by both one- and two-dimensional NMR experiments. The titration was stopped after approximately 1 molar equivalent of calcium had been added. Under these conditions, the linewidths were reasonably narrow without an undue contamination by the $(Ca^{2+})_2$ species (cf. Results). A similar titration ending at a total of 2.5 molar equivalents of added calcium was carried out on another 18 mg apo sample in order to investigate calcium binding to the lower-affinity C-terminal site.

The amide proton exchange rates of $(Ca^{2+})_1$·N56A were examined by lyophilizing the $(Ca^{2+})_1$ sample and redissolving in ^2H_2O (99.96 atom % ^2H; MSD Isotopes). For other experiments acquired from ^2H_2O solution, the sample was lyophilized and redissolved in ^2H_2O (99.996 atom % ^2H; MSD Isotopes) two additional times.

NMR experiments

All NMR experiments were acquired on Bruker AMX-300, AMX-500, or AMX-600 spectrometers at 300 K. Spectra were referenced to the residual H_2O or HO^2H resonance at 4.75 ppm. The following 2D experiments were acquired using standard phase cycling: COSY (Aue et al., 1976), 3QF-COSY (Rance & Wright, 1986), 2Q and 3Q (Braunschweiler et al., 1983), and NOESY (Macura & Ernst, 1980). A composite 180° pulse (Levitt & Freeman, 1979) was used in the middle of the preparation period of the 2Q and 3Q experiments. TOCSY (Braunschweiler & Ernst, 1983) experiments using a DIPSI-2 sequence (Shaka et al., 1988) for isotropic mixing were recorded with the modification described by Rance (1987). NOESY and TOCSY experiments were recorded with a sine modulation in t_1 (Otting et al., 1986) and with a Hahn echo period after the read pulse in order to improve the baseline (Rance & Byrd, 1983; Davis, 1989). Low-power irradiation of the solvent resonance was used during the relaxation delays of 1.2–2.0 s and during the mixing time of the NOESY experiments.

For assignments of apo N56A, a COSY and a NOESY (τ_m = 200 ms) were acquired from a 90% ^1H_2O/10% ^2H_2O solution. Assignments of the $(Ca^{2+})_2$ state were made using NOESY (τ_m = 200 ms), COSY, 2Q (τ_e = 32 ms), and two TOCSY spectra (τ_m = 80, 120 ms) acquired from a 90% ^1H_2O/10% ^2H_2O solution. The $(Ca^{2+})_1$ state was assigned using NOESY (τ_m = 200 ms), COSY, 2Q (τ_e = 32 ms), and two TOCSY spectra (τ_m = 80, 120 ms) acquired from a 90% ^1H_2O/10% ^2H_2O solution, and a NOESY (τ_m = 200 ms), 3Q (τ_e = 22 ms), 3QF-COSY, and two TOCSY spectra (τ_m = 60, 100 ms) collected in ^2H_2O. For amide exchange measurements, a 1D spectrum was acquired 11 min after dissolving in ^2H_2O, followed by a quick (3-h) 2Q experiment with extensive folding in ω_1 at minute 12, another 1D after 3 h 56 min, a full (16-h) 2Q experiment after 3 h 57 min, and a final 1D after 28 h.

Acknowledgments

We thank Professor Sture Forsén for his continued support and collaboration, and Drs. Sara Linse, Mikael Akke, and Göran Carlström for helpful discussions. This work was supported by an operating grant from the National Institutes of Health (GM-40120) and in part by a fellowship to W.J.C. from the American Cancer Society (FRA-436).

References

Akke M, Forsén S, Chazin WJ. 1991. Molecular basis for cooperativity in Ca^{2+} binding to calbindin D_{9k}: ^1H nuclear magnetic resonance studies of $(Cd^{2+})_1$-bovine calbindin D_{9k}. *J Mol Biol 220*:173–189.

Akke M, Forsén S, Chazin WJ. 1995. Three-dimensional solution structure of $(Cd^{2+})1$ calbindin D_{9k} reveals details of the stepwise structural changes along the apo → $(Ca^{2+})_1^{II}$ → $(Ca^{2+})_2^{I,II}$ binding pathway. *J Mol Biol*. Forthcoming.

Akke M, Skelton NJ, Kördel J, Palmer AG, Chazin WJ. 1993. Effects of ion binding on the backbone dynamics of calbindin D_{9k} determined by ^{15}N NMR relaxation. *Biochemistry 32*:9832–9844.

Aue WP, Bartholdi E, Ernst RR. 1976. Two-dimensional spectroscopy: Application to nuclear magnetic resonance. *J Chem Phys 64*:2229–2246.

Beckingham K. 1991. Use of site-directed mutations in the individual Ca^{2+}-binding sites of calmodulin to examine Ca^{2+}-induced conformational changes. *J Biol Chem 266*:6027-6030.

Braunschweiler L, Bodenhausen G, Ernst RR. 1983. Analysis of networks of coupled spins by multiple-quantum N.M.R. *Mol Phys 48*:535-560.

Braunschweiler L, Ernst RR. 1983. Coherence transfer by isotropic mixing: Applications to proton correlation spectroscopy. *J Magn Reson 53*: 521-528.

Brodin P, Drakenberg T, Thulin E, Forsén S, Grundstrom T. 1989. Selective proton labeling of amino acids in deuterated bovine calbindin D_{9k}: A way to simplify ^1H NMR spectra. *Protein Eng 2*:353-358.

Brodin P, Grundström T, Hofmann T, Drakenberg T, Thulin E, Forsén S. 1986. Expression of bovine intestinal CaBP from a synthetic gene in *Escherichia coli* and characterization of the product. *Biochemistry 25*:5371-5377.

Carlström G, Chazin WJ. 1993. Two-dimensional ^1H nuclear magnetic resonance studies of the half-saturated $(Ca^{2+})_1$ state of calbindin D_{9k}: Further implications for the molecular basis of cooperative Ca^{2+} binding. *J Mol Biol 231*:415-430.

Chazin WJ, Kördel J, Thulin E, Hofmann T, Drakenberg T, Forsén S. 1989. Identification of an isoaspartyl linkage formed upon deamidation of bovine calbindin D_{9k} and structural characterization by 2D ^1H NMR. *Biochemistry 28*:8646-8653.

Christakos S, Gabrielides C, Rhoten WB. 1989. Vitamin D-dependent CaBPs: Chemistry, distribution, functional considerations, and molecular biology. *Endocr Rev 10*:3-26.

Davis DG. 1989. Elimination of baseline distortions and minimization of artifacts from phased 2D NMR spectra. *J Magn Reson 81*:603-607.

Forsén S, Kördel J, Grundström T, Chazin WJ. 1993. The molecular anatomy of a CaBP. *Acc Chem Res 26*:7-14.

Gao ZH, Krebs J, VanBerkum MF, Tang WJ, Maune JF, Means AR, Stull JT, Beckingham K. 1993. Activation of four enzymes by two series of calmodulin mutants with point mutations in individual Ca^{2+} binding sites. *J Biol Chem 268*:20096-20104.

Haiech J, Kilhoffer MC, Lukas TJ, Craig TA, Roberts DM, Watterson DM. 1991. Restoration of the calcium binding activity of mutant calmodulins toward normal by the presence of a calmodulin binding structure. *J Biol Chem 266*:3427-3431.

Johansson C, Brodin P, Grundstrom T, Thulin E, Forsén S, Drakenberg T. 1990. Biophysical studies of engineered mutant proteins based on calbindin D_{9k} modified in the pseudo EF-hand. *Eur J Biochem 187*:455-460.

Kördel J, Forsén S, Chazin WJ. 1989. ^1H NMR sequential resonance assignments, secondary structure, and global fold in solution of the major (*trans*-Pro 43) form of bovine calbindin D_{9k}. *Biochemistry 28*:7065-7074.

Kördel J, Forsén S, Drakenberg T, Chazin WJ. 1990. The rate and structural consequences of proline *cis-trans* isomerization in calbindin D_{9k}: NMR studies of the minor (*cis*-Pro 43) isoform and the Pro 43 Gly mutant. *Biochemistry 29*:4400-4409.

Kördel J, Skelton NJ, Akke M, Chazin WJ. 1993. High-resolution solution structure of calcium-loaded calbindin D_{9k}. *J Mol Biol 231*:711-734.

Kraulis P. 1991. MOLSCRIPT: A program to produce both detailed and schematic plots of protein structures. *J Appl Crystallogr 24*:946-950.

Kretsinger RH, Nockolds CE. 1973. Carp muscle calcium binding protein: Structure determination and general description. *J Biol Chem 248*:3313-3326.

Levitt M, Freeman R. 1979. NMR population inversion using a composite pulse. *J Magn Reson 33*:473-476.

Linse S, Brodin P, Drakenberg T, Thulin E, Sellers P, Elmdén K, Grundström T, Forsén S. 1987. Structure-function relationships in EF-hand Ca^{2+}-binding proteins: Protein engineering and biophysical studies of calbindin D_{9k}. *Biochemistry 26*:6723-6735.

Linse S, Chazin WJ. 1995. Quantitative measurements of the cooperativity in an EF-hand protein with sequential calcium binding. *Protein Sci 4*: 1038-1044.

Macura S, Ernst RR. 1980. Elucidation of cross-relaxation in liquids by two-dimensional N.M.R. spectroscopy. *Mol Phys 41*:95-117.

Maune JF, Klee CB, Beckingham K. 1992. Ca^{2+}-binding and conformational change in two series of point mutations to the individual Ca^{2+}-binding sites of calmodulin. *J Biol Chem 267*:5286-5295.

Otting G, Widmer H, Wagner G, Wüthrich K. 1986. Origin of t_1 and t_2 ridges in 2D NMR spectra and procedures for suppression. *J Magn Reson 66*:187-193.

Putkey JA, Sweeney HL, Campbell ST. 1989. Site-directed mutation of the trigger calcium-binding sites in cardiac troponin C. *J Biol Chem 264*: 12370-12378.

Rance M. 1987. Improved techniques for homonuclear rotating-frame and isotropic-mixing experiments. *J Magn Reson 74*:557-564.

Rance M, Byrd RA. 1983. Obtaining high-fidelity spin-1/2 powder spectra in anisotropic media: Phase-cycled Hahn echo spectroscopy. *J Magn Reson 54*:221-240.

Rance M, Wright PE. 1986. Analysis of ^1H-NMR spectra of proteins using multiple-quantum coherence. *J Magn Reson 66*:372-378.

Rasmussen H. 1986a. The calcium messenger system, part I. *N Engl J Med 314*:1094-1101.

Rasmussen H. 1986b. The calcium messenger system, part II. *N Engl J Med 314*:1164-1170.

Rasmussen H. 1989. The cycling of calcium as an intracellular messenger. *Sci Am 261*:66-73.

Shaka AJ, Lee CJ, Pines A. 1988. Iterative schemes for bilinear operators: Application to spin decoupling. *J Magn Reson 77*:274-293.

Skelton NJ, Kördel J, Akke M, Chazin WJ. 1992. Nuclear magnetic resonance studies of the internal dynamics in Apo, $(Cd^{2+})_1$ and $(Ca^{2+})_2$ calbindin D_{9k}. The rates of amide proton exchange with solvent. *J Mol Biol 227*:1100-1117.

Skelton NJ, Kördel J, Akke M, Forsén S, Chazin WJ. 1994. Signal transduction versus buffering activity in Ca^{2+}-binding proteins. *Nature Struct Biol 1*:239-245.

Skelton NJ, Kördel J, Chazin WJ. 1995. Three-dimensional solution structure of apo calbindin D_{9K} determined by NMR spectroscopy. *J Mol Biol. 249*:441-462.

Skelton NJ, Kördel J, Forsén S, Chazin WJ. 1990. Comparative structural analysis of the calcium free and bound states of the calcium regulatory protein calbindin D_{9k}. *J Mol Biol 213*:593-598.

Staun M. 1991. Calbindin-D of human small intestine and kidney. Purification, molecular properties and clinical significance. *Dan Med Bull 38*: 271-282.

Strynadka NC, James MN. 1989. Crystal structures of the helix-loop-helix CaBPs. *Annu Rev Biochem 58*:951-998.

Svensson LA, Thulin E, Forsén S. 1992. Proline *cis-trans* isomers in calbindin D_{9k} observed by X-ray crystallography. *J Mol Biol 223*:601-606.

Szebenyi DME, Moffat K. 1986. The refined structure of vitamin D-dependent CaBP from bovine intestine. *J Biol Chem 261*:8761-8777.

Wagner G. 1983. Characterization of the distribution of internal motions in the basic pancreatic trypsin inhibitor using a large number of internal NMR probes. *Q Rev Biophys 16*:1-57.